https://doi.org/10.5194/essd-2022-277
Preprint. Discussion started: 16 August 2022

Open Access Earth System Science Data Discussions

The global leaf chlorophyll content dataset over 2003–2012 and 2018–2020 derived from MERIS/OLCI satellite data (GLCC): algorithm and validation

Xiaojin Qian[1,2], Liangyun Liu[3,4], Xidong Chen[5], Xiao Zhang[3,4], Siyuan Chen[6], Qi Sun[7]

[1]School of Geographic and Biologic Information, Nanjing University of Posts and Telecommunications, Nanjing, 210023, China
[2]State Key Laboratory of Remote Sensing Science, Aerospace Information Research Institute, Chinese Academy of Sciences. Beijing, 100101, China
[3]International Research Center of Big Data for Sustainable Development Goals, Beijing, 100094, China
[4]Key Laboratory of Digital Earth Science, Aerospace Information Research Institute, Chinese Academy of Sciences, Beijing 100094, China
[5]College of Surveying and Geo-Informatics, North China University of Water Resources and Electric Power, Zhengzhou, 450046, China
[6]College of Geological Engineering and Geomatics, Chang'an University, Xi'an, 710054, China
[7]College of Surveying and Planning, Shangqiu Normal University, Shangqiu, 476000, China

Correspondence to: Liangyun Liu (liuly@radi.ac.cn)

Abstract. Leaf chlorophyll content (LCC), a prominent plant physiological trait and a proxy for leaf photosynthetic capacity, plays a crucial role in the monitoring of agriculture and carbon cycle modeling. In this study, global 500 m LCC weekly dataset (GLCC) for the period 2003–2012 to 2018–2020 were produced from ENVISAT MERIS and Sentinel-3 OLCI satellite data using a physically-based radiative transfer modeling approach. Firstly, five look-up-tables (LUTs) were generated using PROSAIL-D and PROSPECT-D+4-Scale models for woody and non-woody plants, respectively. For the four LUTs applicable to woody plants, each LUT contains three sub-LUTs corresponding to three types of crown height. For the one LUT applicable to non-woody vegetation type, it includes 25 sub-LUTs corresponding to five kinds of canopy structure and five kinds of soil background. The average of the LCC inversion results of all sub-LUTs for each plant function type (PFT) was considered as the retrieval. The LUT algorithm was validated using the synthetic dataset, which gave an R^2 value higher than 0.79 and an RMSE value lower than 10.5 μg cm^{-2}. Then, the GLCC dataset was generated using the MERIS/OLCI multispectral data over 2003–2012 and 2018–2020 at a spatial resolution of 500 m and temporal resolution of one week. The GLCC dataset was validated using 161 field measurements, covering six PFTs. The validation results yielded an overall accuracy of R^2 = 0.41 and RMSE = 8.94 μg cm^{-2}. Finally, the GLCC dataset presented acceptable consistency with the existing MERIS LCC dataset developed by Croft et al. (2020). OLCI, as the successor to MERIS data, was used for the first time to co-produce LCC data from 2003–2012 to 2018–2020 in conjunction with MERIS data. This new GLCC dataset spanning nearly 20 years will provide a valuable opportunity for the monitoring of vegetation growth and terrestrial carbon cycle modeling. The GLCC dataset is available at https://doi.org/10.25452/figshare.plus.20439351 (Qian et al., 2022b).

https://doi.org/10.5194/essd-2022-277
Preprint. Discussion started: 16 August 2022

1 Introduction

Carbon dioxide uptake by terrestrial plants through photosynthesis is the primary driver of multiple global biogeochemical cycles (Badgley et al., 2017; Xiao et al., 2019). Therefore, quantifying photosynthesis on a global scale is fundamental to understanding the global carbon cycle (Ryu et al., 2019). Chlorophyll, as the primary photosynthetic pigment, facilitates the harvesting of energy from light, and the conversion of the light energy into stored chemical energy and thus plays a vital role in the exchange of matter and energy fluxes (Gitelson et al., 2003; Li et al., 2021). Currently, many studies have indicated that leaf chlorophyll content (LCC) is closely related to plant photosynthetic capacity parameter (Vcmax) (Croft et al., 2017; Qian et al., 2021; Wang et al., 2020; Lu et al., 2020; Li et al., 2022). Moreover, leaf chlorophyll content has essential implications on plant physiological status assessment and stress diagnosis (Jay et al., 2017a; Kira et al., 2015; Qian et al., 2022a; Zhang et al., 2021; Jiang et al., 2022; Houborg et al., 2011). As a result, deriving leaf chlorophyll content data over an extensive range of space and time is of great significance in reducing the uncertainty of terrestrial ecosystem productivity and carbon sink estimates (Luo et al., 2019).

Due to the heterogeneity of variations in LCC and the lack of observation that can detect these variations both spatially and temporally, it is not possible to monitor LCC on a global scale using ground-based observations (Piao et al., 2020). Satellite-based remote sensing, through regular global measurements, has enabled continuous estimation of LCC (Croft et al., 2013; Darvishzadeh et al., 2019). The first global LCC dataset was generated using data from ENVISAT MEdium Resolution Imaging Spectrometer (MERIS) based on the physically-based inversion method (Croft et al., 2020). However, MERIS is no longer in operation—it was in operation from 2003 to 2012. As the successor of MERIS, Sentinel-3 Ocean and Land Colour Instrument (OLCI), also launched by the European Space Agency (ESA), will be obliged to succeed MERIS and continue the terrestrial vegetation monitoring mission.

The estimation of the leaf-scale parameter, LCC, from the canopy level remains challenging due to leaf scattering signals may be confounded with the signals of canopy structure and soil background (Jay et al., 2017b; Li et al., 2020; Xu et al., 2019; Houborg et al., 2009; Zarco-Tejada et al., 2005; Zhang et al., 2008). Varieties of vegetation indices (VIs) were developed and widely used to retrieve LCC due to their simplicity and high computational efficiency (Verrelst et al., 2015; Haboudane et al., 2002; Wu et al., 2008; Croft et al., 2014). The development of VIs has gradually clarified the unique value of the red-edge bands and considered reducing its sensitivity to canopy structure and soil background (Sims and Gamon, 2002; Daughtry et al., 2000; Haboudane et al., 2002; Wu et al., 2008; Gitelson et al., 2003; Yin et al., 2022). While VIs models may perform well at the field level, they usually cannot be transferred to other species and regions due to the lack of a clear physical foundation, which depends heavily on the training samples (Croft and Chen, 2017; Sun et al., 2018). In contrast, the physically-based models establish the relationships between the leaf optical properties and the vegetation spectra by simulating interactions of light with the canopy based on radiative transfer theory. The radiative transfer model approach realizes a large number of

https://doi.org/10.5194/essd-2022-277
Preprint. Discussion started: 16 August 2022

vegetation leaf and canopy spectra simulations, that integrates a variety of confounding scene information, and is therefore considered ideal for global LCC mapping (Li et al., 2021). To deal with the ill-posed problems in the retrieval of crop LCC caused by the lack of prior information, a look-up-table (LUT) method that combines multiple types of canopy structure and soil background was proposed in our previous study (Qian and Liu, 2020). However, the feasibility of this algorithm for LCC estimation of other plant function types (PFTs) (e.g., forests and shrubs), is not yet known, as is the applicability of this approach to OLCI satellite data.

In this study, we aimed to generate a global LCC dataset using MERIS and OLCI data from 2003–2012 to 2018–2020 (GLCC) with an improved LUT approach by inverting radiative transfer models. Ground measured data covering six different PFTs were subsequently used to validate the LCC retrievals. In addition, this new LCC dataset was compared to the existing global LCC dataset to analyze its spatial and temporal characteristics. The global leaf chlorophyll content data spanning nearly two decades will contribute to vegetation dynamics monitoring and ecosystem modeling.

2 Data and methods

2.1 Satellite data

2.1.1 MERIS and OLCI surface reflectance data

MERIS full resolution surface reflectance (SR) product and Sentinel-3 SY_2_SYN (synergy) product were selected for generating global LCC product. MERIS SR product provides 7-day synthetic images covering the years from 2003 to 2012. It has 15 spectral bands ranging from the visible to the near-infrared with a resolution of 300 m. The SY_2_SYN product was launched by ESA in October 2018, and integrates the information from the OLCI and Land Surface Temperature Radiometer (SLSTR) on board ESA's Sentinel-3A and Sentinel-3B satellites, including surface reflectance and aerosol parameters over land. OLCI has a 300 m resolution with 21 distinct bands. MERIS and OLCI surface reflectance was used to produce a global LCC dataset, mainly due to the possessing of chlorophyll-sensitive red-edge bands, medium spatial resolution, and a short revisit cycle (Curran and Steele, 2005). The band settings of MERIS and OLCI are shown in Table 1, and the ones in bold are used for LCC retrieval.

Table 1. The channel settings of MERIS and OLCI.

MERIS channel	center (nm)	width (nm)	OLCI channel	center (nm)	width (nm)
			Oa1	400	15
1	412.5	10	Oa2	412.5	10
2	442.5	10	Oa3	442.5	10
3	490	10	Oa4	490	10
4	510	10	Oa5	510	10
5	560	10	Oa6	560	10

https://doi.org/10.5194/essd-2022-277
Preprint. Discussion started: 16 August 2022

6	620	10	Oa7	620	10
7	665	10	Oa8	665	10
			Oa9	673.75	7.5
8	**681.25**	**7.5**	**Oa10**	**681.25**	**7.5**
9	**708.75**	**10**	**Oa11**	**708.75**	**10**
10	**753.75**	**7.5**	**Oa12**	**753.75**	**7.5**
11	760.625	3.75	Oa13	761.25	2.5
			Oa14	764.375	3.75
			Oa15	767.5	2.5
12	778.75	15	Oa16	778.75	15
13	865	20	Oa17	865	20
14	885	10	Oa18	885	10
15	900	10	Oa19	900	10
			Oa20	940	20
			Oa21	1020	40

2.1.2 MODIS land cover map

The MODIS Land Cover Type (MCD12Q1) Version 6 product provides global data with 500 m spatial resolution at annual time steps from 2001 to 2020 (https://doi.org/10.5067/MODIS/MCD12Q1.006). The International Geosphere Biosphere Programme (IGBP) scheme was used in this study, which has 17 land cover types, including 11 natural vegetation types. In this study, these 11 natural vegetation types were combined into five types: needleleaf forests, evergreen broadleaf forests, deciduous broadleaf forests, shrublands and croplands/grasslands.

2.1.3 The Croft MERIS LCC dataset

The 2003–2011 weekly global dataset of LCC was generated by Croft et al. (2020) (referred to as Croft MERIS LCC, hereafter) from MERIS data applying a two-step physically-based approach. For the first step, leaf reflectance was derived from the MERIS SR product using SAIL or 4-Scale canopy radiative transfer models based on the canopy structural characteristics. Secondly, leaf chlorophyll content was inverted from the simulated leaf reflectance generated in the first step based on the PROSPECT-5 leaf radiative transfer model. The Croft MERIS LCC dataset with 300 m spatial resolution was resampled to 500 m to facilitate the comparison with the GLCC dataset generated in this study.

2.2 LCC field measurements

The field LCC data from 161 sampling measurements covering six PFTs were collected to validate the GLCC dataset. The LCC data included 45 observations in deciduous broadleaf forests (DBF), 15 observations in evergreen broadleaf forests (EBF), 48 observations in needleleaf forests (ENF), 21 observations in grasslands (GRA), 29 observations in croplands (CRO), and

https://doi.org/10.5194/essd-2022-277
Preprint. Discussion started: 16 August 2022

three observations in shrublands (SHR). A notable source of these data is the National Ecological Observatory Network (NEON), supported by the National Science Foundation (NSF) funded Grand Challenge project (Keller et al., 2008; Scholl et al., 2020). These sites are covered with relatively homogeneous vegetation at a 500 m scale based on the Google Earth images. For each ground measurement site, the number of samplings and dates are reported in Table 2. The method of LCC measurement was through laboratory chemical analysis.

Table 2. Details of the field measurements of LCC for validation used in this study.

Site name	Latitude	Longitude	PFT	Dominant species	Sampling date	Samples	Reference/Source
Sudbury_DBF	47.16	−81.71	DBF	Trembling aspen	Summer 2007	2	Simic et al. (2011)
Haliburton	45.24	−78.54	DBF	Sugar maple	May–Sep 2004	8	Zhang et al. (2007)
JERC_DBF	31.19	−84.47	DBF	Southern red oak	Sep 2019	7	National Ecological Observatory (2022)
UNDE	46.23	−89.54	DBF	Red and sugar maple, aspen, paper birch	Jun 2019	8	
DELA	32.54	−87.81	DBF	Oak, hickory	Apr–May 2019	4	
CLBJ_DBF	33.40	−97.59	DBF	Post oak, blackjack oak	Apr–May 2019	13	
BONA	65.16	−147.54	DBF	-	Jul–Aug 2019	3	
SJER_EBF	37.11	−119.73	EBF	Evergreen oak	Mar–Apr 2019	8	
PUUM	19.56	−155.30	EBF	'Ohi'a lehua	Jan 2019	7	
Sudbury_Simic	47.18	−81.74	ENF	Black spruce	Summer 2007	5	Simic et al. (2011)
Sudbury_Zhang	47.16	−81.74	ENF	Black spruce	Summer 2003–2004	16	Zhang et al. (2008)
JERC_ENF	31.20	−84.46	ENF	Longleaf pine	Sep 2019	9	National Ecological Observatory (2022)
NIWO_ENF	40.04	−105.56	ENF	lodgepole pine	Aug 2019	6	
WREF	45.83	−121.97	ENF	Douglas fir, western hemlock, pacific silver fir	Jul 2019	12	
CLBJ_GRA	33.37	−97.58	GRA	Bluestem	Apr–May 2019	6	
NIWO_GRA	40.05	−105.58	GRA	Curly sedge	Aug 2019	3	
SJER_GRA	37.10	−119.73	GRA	Bromus	Mar–Apr 2019	12	
US-Ne2	41.17	−96.47	CRO	Soybean	Jun–Sep 2004	21	University of Nebraska–Lincoln
KONA	39.13	−96.63	CRO	Wheat, corn	Jul 2019	8	National Ecological Observatory (2022)
NIWO_SHR	40.05	−105.59	SHR	-	Aug 2019	1	
SJER_SHR	37.11	−119.75	SHR	Manzanita, whitethorn shrub	Mar–Apr 2019	2	

https://doi.org/10.5194/essd-2022-277
Preprint. Discussion started: 16 August 2022

2.3 The cross-validation sites

The site location information from the FLUXNET2015 dataset was extracted for the cross-validation between the Croft MERIS LCC dataset and the GLCC dataset. Considering the spatial-temporal consistency of satellite products, we selected 178 sites for the validation of the GLCC dataset in this study. The ground measured sites in Table 2, the selected 178 cross-validation sites, and the IGBP land cover map are shown in Fig. 1.

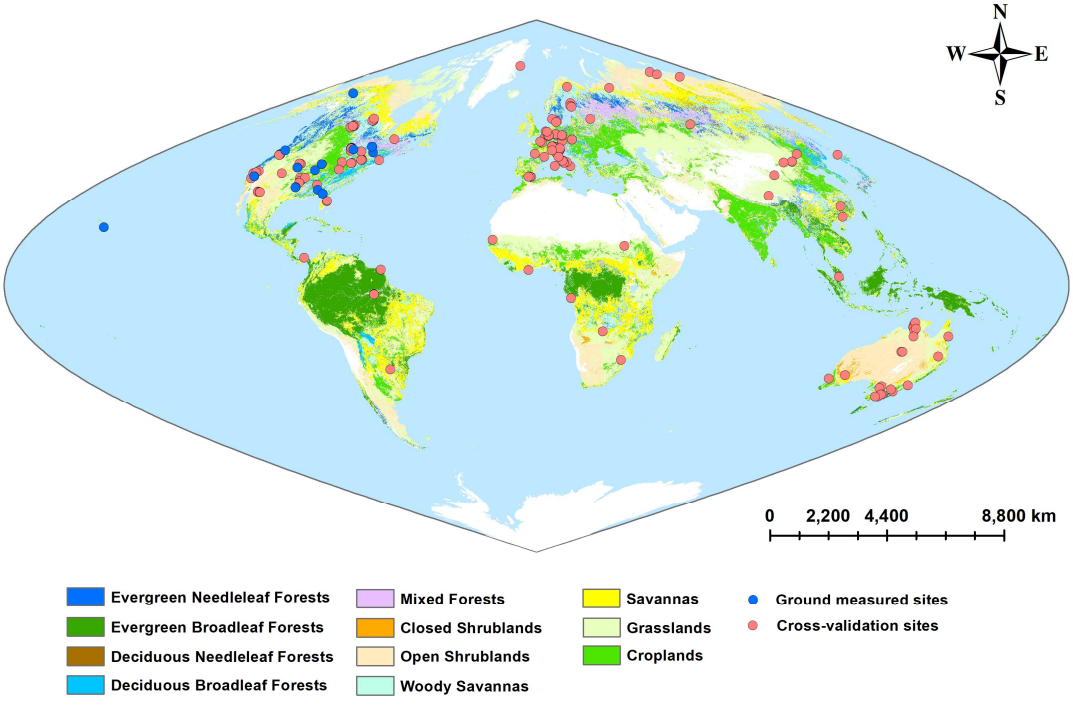

Figure 1. Global MCD12Q1 land cover map and the locations of the ground measured sites and the cross-validation sites for the validation of the GLCC dataset.

2.4 Algorithm development

An improved LUT approach was selected to derive LCC from satellite data on a global scale. This LUT-based inversion approach has been successfully work in the retrieval of crop LCC (Qian and Liu, 2020). In this study, the 4SAIL canopy bidirectional reflectance model (Verhoef et al., 2007) and 4-Scale geometric-optical model (Chen and Leblanc, 1997) combined with the PROSPECT-D leaf optical properties model (Féret et al., 2017), were used to simulate the homogenous

https://doi.org/10.5194/essd-2022-277
Preprint. Discussion started: 16 August 2022

and heterogeneous canopy reflectance spectra, respectively. It should be noted that canopy spectra were convolved with spectral response functions to match the MERIS and OLCI bands.

2.4.1 Canopy reflectance modeling – PROSPECT-D and 4SAIL model

It is known that turbid medium models such as 4SAIL are a poor representation of heterogeneous and structurally complex canopies since they assume a random distribution of leaves. Thus, the 4SAIL model was used to simulate the canopy spectra for homogenous canopies, such as crops and grasses. Table 3 shows the input parameters within the PROSPECT-D and 4SAIL model. At the leaf level, only LCC varied, with a range of 10–80 μg cm^{-2}. At the canopy level, the leaf inclination distribution function (LIDF) was set to five commonly used types except for the erectophile distribution because of the underestimation of LCC with the consideration of erectophile distribution (Qian and Liu, 2020). LAI was set from 0.25 to 8 to model the scenarios with different levels of vegetation cover. The soil reflectance was determined by multiplying the field-measured dry and bare soil spectra by five different brightness coefficients (Fig. 2). The solar zenith angle was set from 0° to 60°, with a step of 10°. An LUT was then generated, which contained 25 sub-LUTs corresponding to five kinds of canopy structure and five kinds of soil background.

Table 3. The PROSPECT-D and 4SAIL input parameters for LUT generation.

	Input parameters	Value/source
PROSPECT-D	Leaf structural parameter (N)	1.5
	Leaf chlorophyll content (LCC, μg cm^{-2})	10–80, step 10
	Leaf carotenoid content (C_{xc}, μg cm^{-2})	LCC/4
	Equivalent water thickness (C_w, cm)	0.02
	Dry matter content (C_m, g cm^{-2})	0.004
	Leaf anthocyanin content (C_{anth}, μg cm^{-2})	2
	Leaf brown pigment content (C_{bp})	0
4SAIL	leaf inclination distribution function	[1,0], [0,−1], [0,1], [−0.35,0.15], [0,0]
	Leaf area index (LAI)	0.25, 0.5, 0.75, 1, 1.25, 1.5, 1.75, 2, 3, 4, 5, 6, 7, 8
	Hot spot parameter (S_L)	0.05
	Soil reflectance (ρ_s)	As shown in Fig. 2
	Solar zenith angle (θ_s, °)	0, 10, 20, 30, 40, 50, 60
	View zenith angle (θ_v, °)	0
	Relative azimuth angle (φ, °)	0

[1,0], planophile; [0,−1], plagiophile; [0,1], extremophile; [−0.35,−0.15], spherical; [0,0], uniform

https://doi.org/10.5194/essd-2022-277
Preprint. Discussion started: 16 August 2022

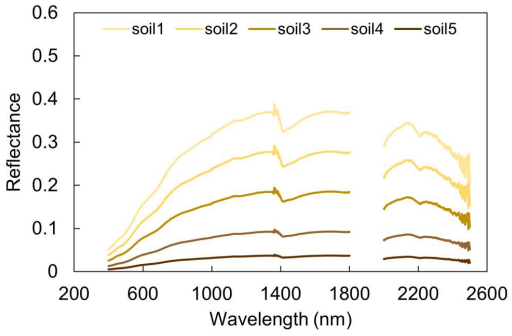

Figure 2. Soil reflectance used in the 4SAIL model. Soil1 reflectance is obtained from the field measured. The others are the soil1 spectrum multiplied by different brightness coefficients.

2.4.2 Canopy reflectance modeling – PROSPECT-D and 4-Scale model

The 4-Scale model was selected to simulate forested and spatially clumped canopy spectra. The significant parameters include tree density, tree height (stick and crown), LAI, crown diameter, crown shape, tree group size, branches and shoots, background soil factor, viewing geometry, and leaf optical properties. Firstly, leaf optical properties were modeled in the PROSPECT-D model based on the values from Table 4 (Croft et al., 2020; Sun et al., 2021b). Then, the 4-Scale model was run to simulate canopy spectra using tree architecture, canopy structure, imaging geometry, and leaf/background properties, as shown in Table 5 (Chen and Leblanc, 1997; Chen et al., 2005; Chen and Leblanc, 2001). At given viewing geometry, variations of crown height presented an impact on the modeled canopy reflectance and LCC (Zhang et al., 2008; Croft et al., 2020). The 4-Scale model was run in the forward mode to generate four LUTs used to retrieve LCC in DBF, EBF, ENF, and SHR ecosystems, respectively. Each LUT, including three sub-LUTs, was contained to consider three types of crown height.

Table 4. The PROSPECT-D input parameters for the simulation of leaf spectra.

	DBF	EBF	ENF	SHR
LCC (μg cm^{-2})	10–80, step 10	10–80, step 10	10–80, step 10	10–80, step 10
N	1.2	1.8	2.5	1.8
C_{ar} (μg cm^{-2})	LCC/7	LCC/7	LCC/7	LCC/7
C_{anth} (μg cm^{-2})	1	1	1	1
C_{bp}	0	0	0	0
C_m (g cm^{-2})	0.005	0.005	0.035	0.005
C_w (cm)	0.01	0.01	0.048	0.01

https://doi.org/10.5194/essd-2022-277
Preprint. Discussion started: 16 August 2022

165 **Table 5. The 4-Scale input parameters for LUT generation.**

	Broadleaf trees	Needleleaf trees	Shrubland
Stand density (trees/ha)	1000, 2000, 3000, 4000	1000, 2000, 3000, 4000, 6000, 8000, 12000	1000, 2000, 3000, 4000
Leaf area index (m^2 m^{-2})	0.5, 1, 2, 4, 6, 8	0.5, 1, 2, 4, 6, 8	0.5, 1, 2, 4, 6, 8
Stick height (m)	1, 5, 10	1, 5, 10	1, 2, 3
Crown height (m)	5, 10, 20	5, 10, 20	1, 2, 3
Crown radius (m)	0.75, 1, 1.25, 1.5	0.5, 0.75, 1, 1.25	0.75, 1, 1.25, 1.5
Crown shape	Spheroid	Cone & cylinder	Spheroid
Clumping index (ΩE)	0.6, 0.9	0.5, 0.8	0.6, 0.9
Solar zenith angle (°)	10–70, step 10	10–70, step 10	10–70, step 10
View zenith angle (°)	0	0	0
Relative azimuth angle (°)	0	0	0
Neyman grouping	1, 2, 3	1, 2, 3	1, 2, 3
Needle to shoot ratio (γE)	1	1.41	1
Background composition	Green vegetation and soil	Green vegetation and soil	Dry grasses and soil

2.4.3 Deriving leaf chlorophyll content

MERIS and OLCI surface reflectance data were reprojected and resampled to be consistent with the MCD12Q1 product. For DBF and MF PFTs, the DBF LUT, containing three sub-LUTs, corresponding to three types of crown height presented in
170 Table 5, was used. In the processing of inversion using a physically-based model, the inversion results are not always unique, as different combinations of canopy and leaf parameters may produce almost similar spectra (Si et al., 2012). It has been indicated that using prior knowledge is an effective way to deal with this problem and facilitate LCC retrieval (Sun et al., 2021a; Li et al., 2021). The DBF LUT for retrieving DBF and MF LCC from MERIS/OLCI reflectance was optimized based on sun-view geometry that could be available from each satellite image. The root mean square error (RMSE) between
175 MERIS/OLCI canopy reflectance and simulated canopy reflectance was calculated to derive the LCC value for each sub-LUT. Instead of selecting the best spectrum (case) obtained for the smallest RMSE value and its corresponding LCC as the solution, the situation of multiple best cases and the mean of their corresponding LCC values were considered. A different number of cases (the first 1, 10, 50, 100, 500, and 1000 best fits) were conducted in the solution in retrieving LCC. It was found that the average of the best ten solutions yielded the lowest RMSE for the LCC retrieval and served as the retrieval for each sub-LUT.
180 The final inversion result was obtained by averaging the retrievals of the three sub-LUTs by considering multiple types of crown height. The retrieval of LCC for the other PFTs referred to the inversion process described above. It is worth noting that

https://doi.org/10.5194/essd-2022-277
Preprint. Discussion started: 16 August 2022

the four PFTs, WSA, SAV, GRA, and CRO, used the LUT, containing 25 sub-LUTs, established by the PROSAIL_D model. An analysis toward multiple solutions (selecting the first 1, 3, 5, 8, 10, or 15 best fits) was also conducted in each sub-LUT. According to the test by Qian and Liu (2020), the mean of the eight best solutions yielded the best result, and the mean of the retrievals for 25 sub-LUTs was taken as the final retrieval. Multiple averages will reduce the ill-posed inversion problem and improve the robustness of the inversion method. For invalid pixels (reflectance less than 0) and non-vegetated pixels in the MERIS/OLCI data, the LCC value was set to 0.

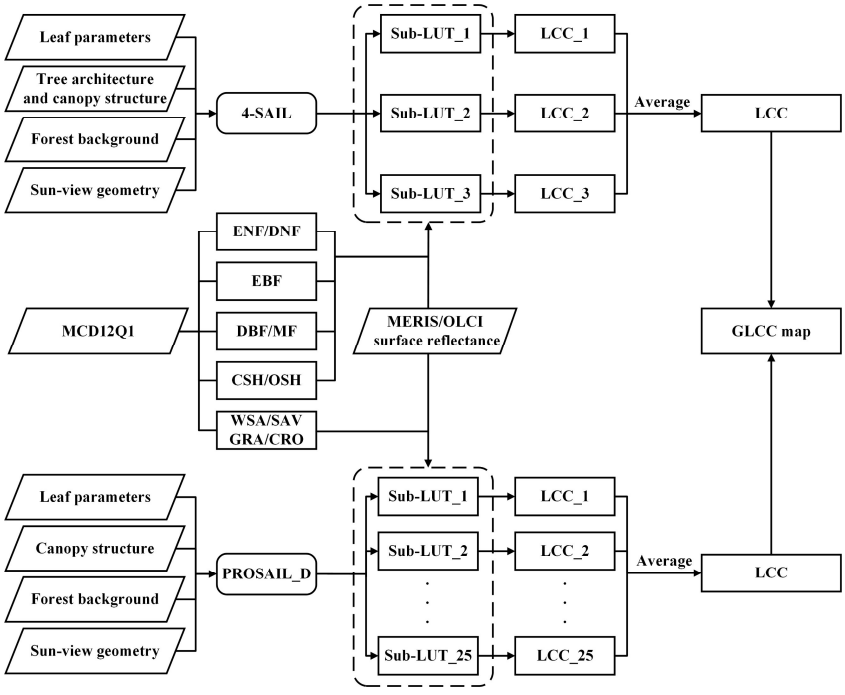

Figure 3. The flowchart of the LUT algorithm to generate GLCC dataset based on 4-Scale and PRPSAIL_D models, respectively.

2.5 Validation and evaluation of the GLCC dataset

The GLCC dataset was validated by comparing it with the collected LCC field measurements comprising 161 field samples over six PFTs in Section 2.2. In addition to field data validation, the GLCC dataset was evaluated from two other aspects: first, to analyze the spatial and temporal variations of the global LCC maps; second, to compare the new LCC dataset with the Croft MERIS LCC dataset at the cross-validation sites

https://doi.org/10.5194/essd-2022-277
Preprint. Discussion started: 16 August 2022

Open Access Earth System Science Data Discussions

3 Results and discussion

3.1 Validation of LUT algorithms for LCC inversion using the synthetic dataset

A random 10% of the synthetic dataset was used to validate the inversion performances of the improved LUT algorithm on the five PFTs (Fig. 4). All the LUT algorithms had R^2 values higher than 0.79 and RMSE values lower than 10.5 μg cm^{-2}. The LUT algorithm for SHR PFT achieved the highest R^2 (about 0.98) and lowest RMSE (2.8 μg cm^{-2}). Except for the DBF and EBF PFTs, the difference in LCC inversion performance of the LUT algorithm on the MERIS and OLCI synthetic datasets is negligible, indicating the applicability and effectiveness of the improved LUT algorithm for MERIS and OLCI satellite data.

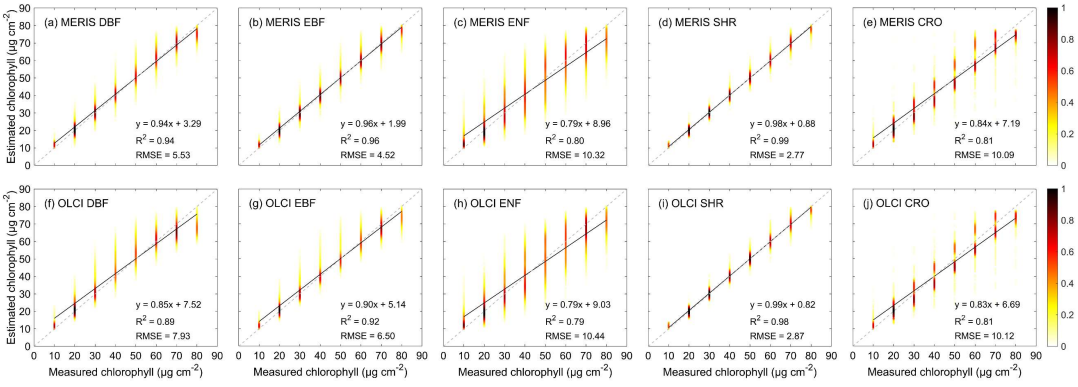

Figure 4. Performances of LCC inversion with the synthetic dataset using the LUT algorithms. Darker colors indicate higher dot density.

3.2 Validation of the GLCC dataset using field measurements

The LCC estimates against ground measured values were plotted in Fig. 5 for all FPTs and Fig. 6 for individual PFTs. With all PFTs combined, the GLCC dataset yielded a relatively good overall accuracy, with a coefficient of determination (R^2) value of 0.41, an RMSE value of 8.94 μg cm^{-2}, and a normalized RMSE (NRMSE=RMSE/range) value of 16.9%. In the case of considering single PFT alone, EBF performed best (R^2=0.61; RMSE=8.03 μg cm^{-2}) followed by DBF (R^2=0.43; RMSE=8.21 μg cm^{-2}) and ENF (R^2=0.32; RMSE=8.09 μg cm^{-2}). The other three PFTS showed similar levels of performance, where RMSE values were 10.58, 10.48, and 7.37 μg cm^{-2} for CRO, GRA, and SHR, respectively. Overall, all PFTs achieved RMSE < 10.6 μg cm^{-2}.

https://doi.org/10.5194/essd-2022-277
Preprint. Discussion started: 16 August 2022

Open Access Earth System Science Data Discussions

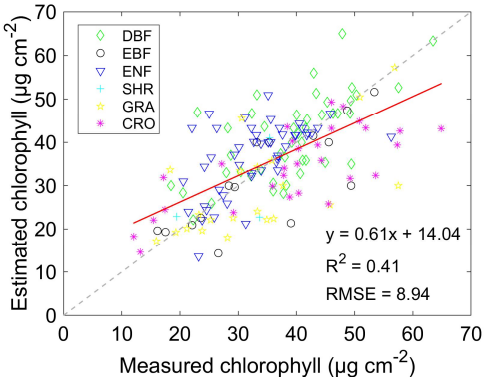

Figure 5. Validation of the GLCC dataset with field measurements for all PFTs.

220

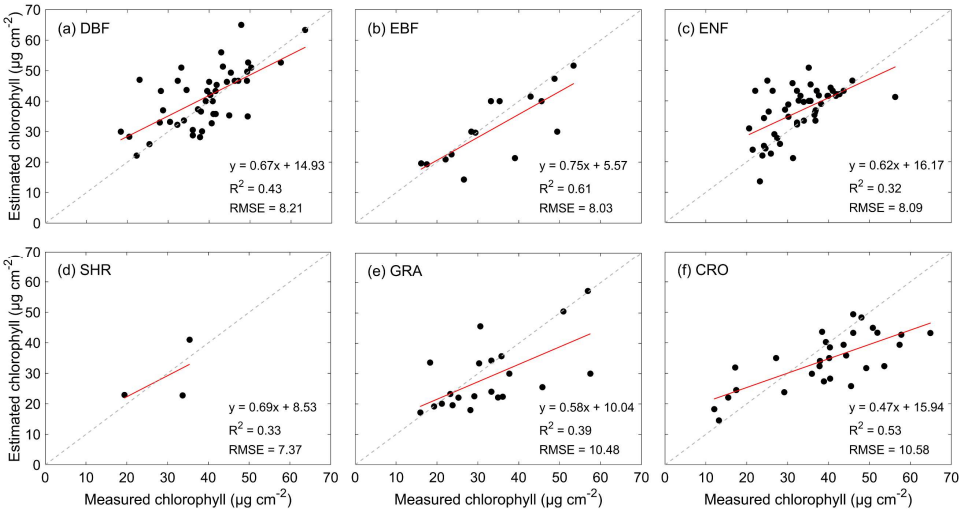

Figure 6. Validation of the GLCC dataset with field measurements for six individual PFTs.

3.3 Spatial and temporal trends in global leaf chlorophyll content

225 The annual global distribution of LCC from OLCI data is presented in Fig. 7(a). The tropical forests in the Congo basin, Amazon region, and Southeast Asia achieved the highest mean LCC values higher than 40 μg cm^{-2}. DBF had relatively high

https://doi.org/10.5194/essd-2022-277
Preprint. Discussion started: 16 August 2022

values of annual mean LCC (about 40 μg cm^{-2}), while GRA had the lowest mean LCC values lower than <30 μg cm^{-2}. The annual mean LCC values of SHR decreased with increasing latitude and did not present a fixed range of values. Fig. 7(b) demonstrates the variation of annual mean LCC with latitude on a global scale. In general, the annual mean LCC value decreased with increasing latitude, which is in line with the general pattern of plant growth.

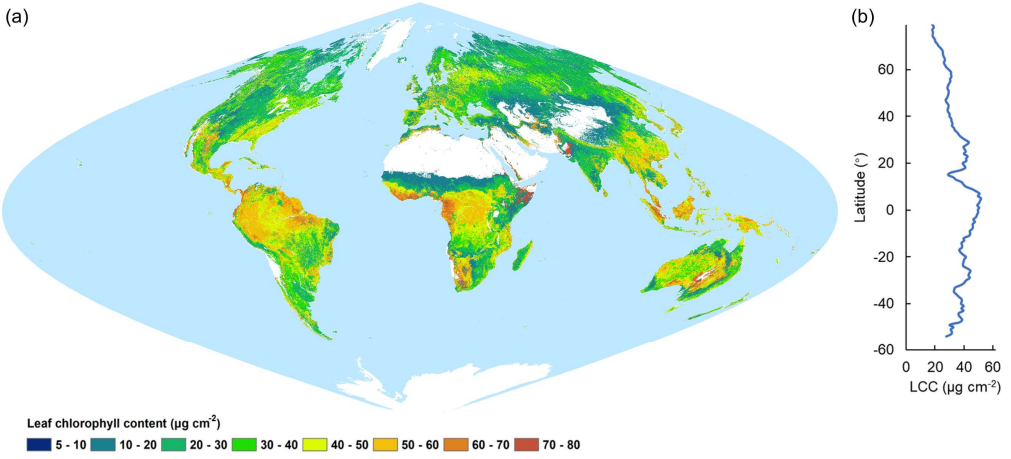

Figure 7. (a) The global annual mean map of GLCC in 2019 and (b) the mean values along latitudinal bands.

The seasonal dynamics in MERIS LCC and OLCI LCC are shown in Fig. 8. The year 2009 and 2019 were divided into two seasons according to the vegetation status and climate in the northern hemisphere, i.e., a growing season from May to October and a non-growing season in the remaining six months. It can be observed that the OLCI LCC map showed a similar overall spatial distribution to the MERIS LCC map, in both the growing and the non-growing seasons, but with richer spatial details. This indicates that the improved LUT algorithm can be well applied to OLCI data, and the dataset has the capacity to represent the LCC spatial distribution. In tropical rainforest areas, LCC remained high all year round. Distinct seasonal variations of LCC were found at the middle and high latitudes of the northern hemisphere. Boreal forests at high latitudes had higher LCC than other PFTs, especially in the growing season. Apparent seasonal variations were found in shrublands in south Africa and Australia.

https://doi.org/10.5194/essd-2022-277
Preprint. Discussion started: 16 August 2022

Open Access Earth System Science Data Discussions

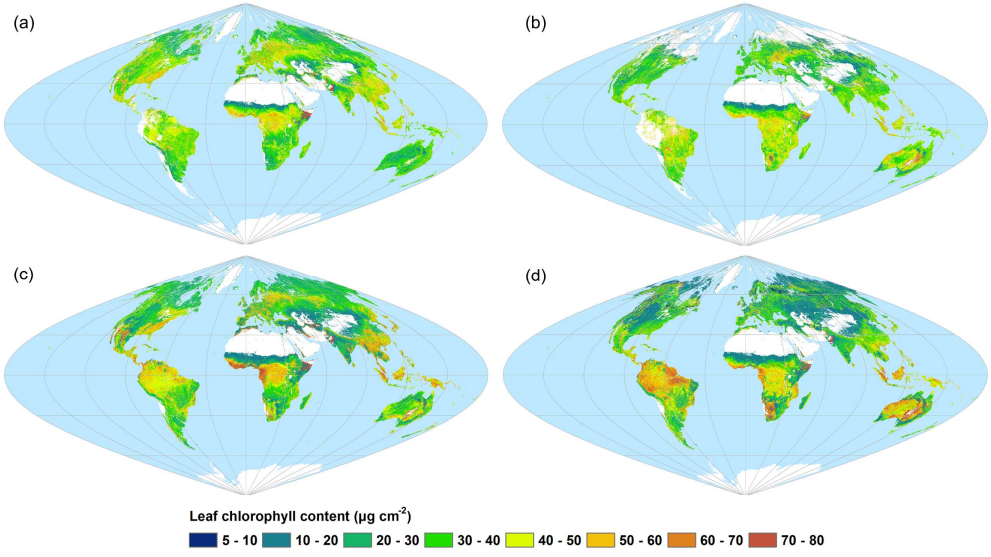

Figure 8. Spatial distribution of the mean LCC using MERIS and OLCI data in the different seasons: (a) and (b) are the mean LCC map using MERIS data in 2009 during the growing and non-growing season for the northern hemisphere, respectively; (c) and (b) are the mean LCC map using OLCI in 2019 during the growing and non-growing season for the northern hemisphere, respectively.

3.4 Comparisons of GLCC dataset and Croft MERIS LCC dataset

The comparisons of GLCC with the Croft MERIS LCC dataset in different PFTs at the cross-validation sites were presented in Fig. 9. The former had narrower value ranges of LCC (generally 10–80 μg cm^{-2}) than the latter (1–90 μg cm^{-2}). The GLCC had higher values than Croft MERIS LCC for DBF and ENF, with RMSE values of 15.28 and 15.44 μg cm^{-2}. The two LCC dataset values were closer for EBF and SHR, with RMSE values of 12.11 and 11.78 μg cm^{-2}. The correlation between GLCC and Croft MERIS LCC was very poor for GRA and CRO, with $R^2 < 0.05$ and RMSE close to 17 μg cm^{-2}. For GRA, the poor correlation was due to the fact that GLCC had lower values than Croft MERIS LCC, while for CRO, it was attributed to the high-density range of GLCC values (20–50 μg cm^{-2}) corresponding to an extensive range of Croft MERIS LCC values (12–60 μg cm^{-2}). In general, the GLCC using the improved LUT method was found to have an acceptable correlation with the Croft MERIS LCC, with an overall accuracy of R^2=0.21, RMSE=15.62 μg cm^{-2}.

https://doi.org/10.5194/essd-2022-277
Preprint. Discussion started: 16 August 2022

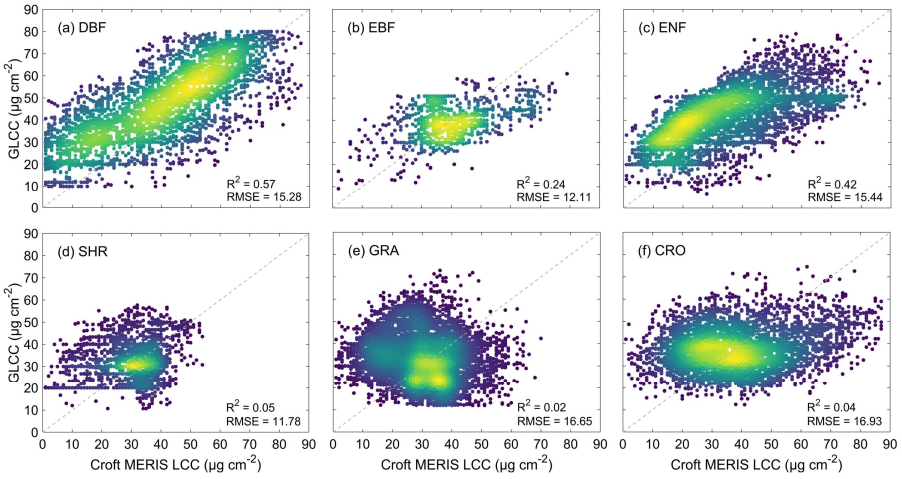

Figure 9. Comparisons of GLCC and Croft MERIS LCC in six different PFTs at the cross-validation sites.

Figure 10 shows the seasonal variations of the two LCC datasets for six different PFTs across the northern hemisphere. The two LCC datasets had the most stable seasonal variations in SHR, with the LCC value range of 20 to 40 μg cm^{-2} all year round. The GLCC presented a slight seasonal variation in comparison with Croft MERIS LCC. The GLCC seasonal trajectories in EBF were relatively consistent across the year, while the Croft MERIS LCC values varied strongly and had chaotic seasonal variations. For ENF, the two datasets had the most similar seasonal trends, while GLCC had higher LCC values than Croft MERIS LCC datasets. In DBF, the two LCC datasets presented apparent seasonal variations and the same peak, but GLCC showed higher values in winter, spring and autumn. The reason may be that the DBF validation sites at middle latitudes had different phenology from those at high latitudes. For GRA, GLCC has more elevated and later peak than Croft MERIS LCC, with more obvious seasonal variations. The seasonal variation of the two datasets in CRO showed opposite trends, except in summer. The GLCC had upward trend in winter and a little peak in summer. This may be due to the lack of LCC data, as only 19 sites were involved in the statistical analysis. The results above confirmed the seasonal variation patterns of the GLCC, especially for SHR and GRA.

https://doi.org/10.5194/essd-2022-277
Preprint. Discussion started: 16 August 2022

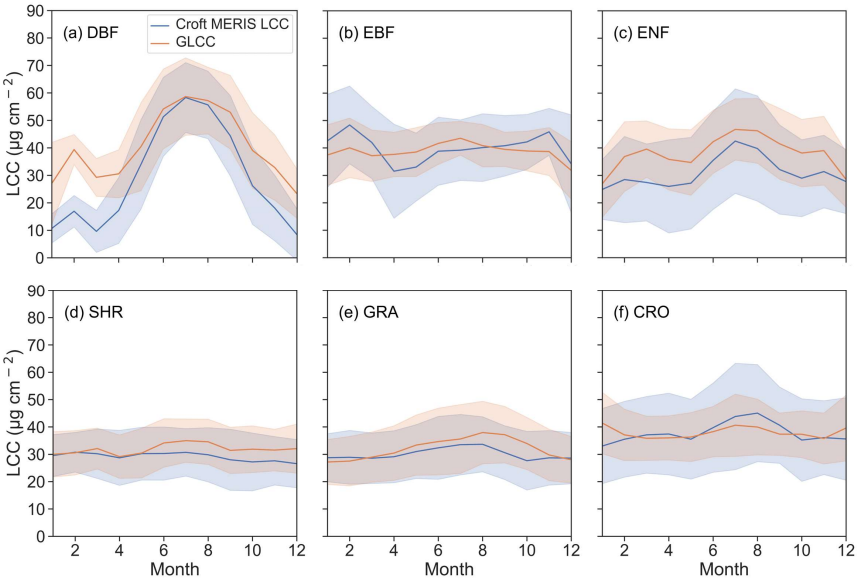

Figure 10. The mean seasonal profiles of the two LCC datasets in six different PFTs at the cross-validation sites in the northern hemisphere. The shadow areas in each subfigure represent one standard deviation.

3.5 Uncertainty in the GLCC dataset

This study is the first to produce a global leaf chlorophyll content dataset using MERIS and OLCI satellite data spanning nearly 20 years from 2003–2012 to 2018–2020, which is of great significance for the study of global change. The overall validation results of the global GLCC dataset were considered within reasonable limits according to the literature (Croft et al., 2020), with an overall accuracy of 8.94 μg cm^{-2} for all PFTs. The limitations and uncertainties in the dataset are the results of factors related to the data used, the model itself, and the validation process.

As only MERIS and OLCI surface reflectance and MCD12Q1 land cover type were involved in the generating of LCC, the accuracy of the GLCC dataset is entirely dependent on the two satellite data without considering the algorithm accuracy. Uncertainties in MERIS and OLCI surface reflectance products may arise from radiometric, geometric, and BRDF corrections as well as atmospheric corrections (Garrigues et al., 2008). In addition, a pixel at the 300 m or 500 m resolution could be affected by pixel heterogeneity, leading to spatial heterogeneity in the vegetation parameter products obtained from the inversion as well (Croft et al., 2013). The effect of pixel heterogeneity on the LUT inversion of LCC requires further evaluation.

https://doi.org/10.5194/essd-2022-277
Preprint. Discussion started: 16 August 2022

Vegetation canopy structure and soil background are two parameters attracting the most attention in this study. In addition, LAI parameters, which can represent vegetation cover to some extent, should also be highly considered. Numerous studies have shown that due to the interference of soil background, the retrieval accuracy of LCC is low under sparse vegetation (Zarco-Tejada et al., 2019; Xu et al., 2019; Croft et al., 2020; Li et al., 2021). How to eliminate the influence of soil background and improve the retrieval accuracy of LCC under sparse vegetation by remote sensing is an urgent scientific question worthy of deep investigation. In generating LUT, some biochemical and structural parameters were fixed as constants according to the PFT separately, which have more or less influence on the simulation of canopy reflectance. Since remote sensing inversion based on a physical model is an ill-posed problem, a trade-off between the universality and computational efficiency of the model and the accuracy of model inversion should be considered.

There are also limitations to the validation of the GLCC dataset. First, the lack of LCC field measurements with seasonal variations across different PFT resulted in insufficient validation on a global scale, particularly for SHR, EBF, and GRA PFTs. Second, the LCC validation across different PFTs using data from independent field campaigns. Nevertheless, it depends on the number of measurements, the measuring position of the leaf, and details of chlorophyll extraction. Although they have all been adequately validated individually, they may still introduce some uncertainty in the validation if putting them together in a raw way. Third, although we have paid attention to the spatial homogeneity of the field sites and tried to select areas with homogeneity within 500 m, the scale problem still exists. It is desirable that ground measured data can be upscaled using high resolution data and then used to validate the LCC dataset.

4 Conclusions

This study generated a new global LCC dataset based on MERIS and OLCI data using an improved LUT method. For grasslands and crops, an LUT, including 25 sub-LUTs, was generated using the PROSAIL model. The final LCC retrievals are the mean values of the 25 sub-LUTs. For forests and shrubs, four LUTs were constructed using PROSPECT-D and 4-Scale models, applicable for evergreen needleleaf forest, evergreen broadleaf forest, deciduous broadleaf forest, and shrubs, respectively. Each LUT contains three sub-LUTs, and the final inversion result is the average value of them. The LUT algorithm was tested using the simulated spectra, which yielded an R^2 value higher than 0.79 and RMSE value lower than 10.5 μg cm^{-2}. The global GLCC dataset was validated and evaluated by comparing with collected field measurements and existed LCC dataset. The GLCC dataset showed good relationships with ground measured data, with an overall accuracy of $R^2 = 0.41$ and RMSE = 8.94 μg cm^{-2}, and presented relatively good consistency with the existing MERIS LCC dataset. The global 7-day LCC data at 500 m resolution from 2003–2012 to 2018–2020 will make an essential step towards analyzing vegetation physiological dynamics and carbon cycle modeling in global change.

https://doi.org/10.5194/essd-2022-277
Preprint. Discussion started: 16 August 2022

Data availability. The global 7-day leaf chlorophyll content data at 500 m resolution from 2003–2012 to 2018–2020 is free to access at https://doi.org/10.25452/figshare.plus.20439351 (Qian et al., 2022b). The global dataset is stored in GeoTIFF format, named "ESACCI-LC-L3-SR-MERIS-500m-P7D-h**v**-YYYYMMDD-v2.0-MODISTile-LCC.tif" and "S3_YYYYMMDD_h**v**_7DaySR-MODISTile-LCC.tif" for MERIS LCC dataset and OLCI LCC dataset, respectively, where "h**v**" is referenced to the MODIS tile. The scale factor of the data is 0.01.

Author contributions. LL conceptualized the project. XQ performed the investigation. LL, XQ and XZ designed the methodology. XC and SC developed the software. XQ and QS performed the validation. XQ prepared the original draft of the paper. LL reviewed and edited the paper.

Acknowledgments. This research was supported by the Innovative Research Program of the International Research Center of Big Data for Sustainable Development Goals (Grant No. CBAS2022IRP01), the National Natural Science Foundation of China (Grant No. 41825002), Open Fund of State Key Laboratory of Remote Sensing Science (Grant No. OFSLRSS202216), and the Natural Science Research Start-up Foundation of Recruiting Talents of Nanjing University of Posts and Telecommunications (Grant No. NY221145). The authors thank all the authors who published the field measurement data cited in this paper, and thank Holly Croft for providing the published field data collection. The authors appreciate the field measurement data provided by the Center for Advanced Land Management Information Technologies (CALMIT), the University of Nebraska–Lincoln, and the National Science Foundation's National Ecological Observatory Network (NEON). The authors thank Jianhua Yang and Dong Li for their help with data processing.

Competing interests. The authors declare that they have no conflict of interest.

References

Badgley, G., Field, C. B., and Berry, J. A.: Canopy near-infrared reflectance and terrestrial photosynthesis, Science Advances, 3, e1602244, https://doi.org/10.1126/sciadv.1602244, 2017.

Chen, J. M. and Leblanc, S. G.: A four-scale bidirectional reflectance model based on canopy architecture, IEEE Transactions on Geoscience and Remote Sensing, 35, 1316-1337, https://doi.org/10.1109/36.628798, 1997.

Chen, J. M. and Leblanc, S. G.: Multiple-scattering scheme useful for geometric optical modeling, IEEE Transactions on Geoscience and Remote Sensing, 39, 1061-1071, https://doi.org/10.1109/36.921424, 2001.

Chen, J. M., Menges, C. H., and Leblanc, S. G.: Global mapping of foliage clumping index using multi-angular satellite data, Remote Sensing of Environment, 97, 447-457, https://doi.org/10.1016/j.rse.2005.05.003, 2005.

Croft, H. and Chen, J. M.: Leaf pigment content, 2017.

Croft, H., Chen, J. M., and Zhang, Y.: The applicability of empirical vegetation indices for determining leaf chlorophyll content over different leaf and canopy structures, Ecological Complexity, 17, 119-130, https://doi.org/10.1016/j.ecocom.2013.11.005, 2014.

https://doi.org/10.5194/essd-2022-277
Preprint. Discussion started: 16 August 2022

Croft, H., Chen, J. M., Zhang, Y., and Simic, A.: Modelling leaf chlorophyll content in broadleaf and needle leaf canopies from ground, CASI, Landsat TM 5 and MERIS reflectance data, Remote Sensing of Environment, 133, 128-140, https://doi.org/10.1016/j.rse.2013.02.006, 2013.

Croft, H., Chen, J., Luo, X., Bartlett, P., Chen, B., and Staebler, R. M.: Leaf chlorophyll content as a proxy for leaf photosynthetic capacity, Global Change Biology, 23, 3513-3524, https://doi.org/10.1111/gcb.13599, 2017.

Croft, H., Chen, J. M., Wang, R., Mo, G., Luo, S., Luo, X., He, L., Gonsamo, A., Arabian, J., and Zhang, Y.: The global distribution of leaf chlorophyll content, Remote Sensing of Environment, 236, 111479, https://doi.org/10.1016/j.rse.2019.111479, 2020.

Curran, P. J. and Steele, C. M.: MERIS: The re-branding of an ocean sensor, International Journal of Remote Sensing, 26, 1781-1798, https://doi.org/10.1080/01431160412331330275, 2005.

Darvishzadeh, R., Skidmore, A., Abdullah, H., Cherenet, E., Ali, A., Wang, T., Nieuwenhuis, W., Heurich, M., Vrieling, A., and O'Connor, B.: Mapping leaf chlorophyll content from Sentinel-2 and RapidEye data in spruce stands using the invertible forest reflectance model, International Journal of Applied Earth Observation and Geoinformation, 79, 58-70, https://doi.org/10.1016/j.jag.2019.03.003, 2019.

Daughtry, C. S. T., Walthall, C. L., Kim, M. S., De Colstoun, E. B., and McMurtrey Iii, J. E.: Estimating corn leaf chlorophyll concentration from leaf and canopy reflectance, Remote Sensing of Environment, 74, 229-239, https://doi.org/10.1016/S0034-4257(00)00113-9, 2000.

Féret, J. B., Gitelson, A. A., Noble, S. D., and Jacquemoud, S.: PROSPECT-D: Towards modeling leaf optical properties through a complete lifecycle, Remote Sensing of Environment, 193, 204-215, https://doi.org/10.1016/j.rse.2017.03.004, 2017.

Garrigues, S., Lacaze, R., Baret, F. J. T. M., Morisette, J. T., Weiss, M., Nickeson, J. E., Fernandes, R., Plummer, S., Shabanov, N. V., and Myneni, R. B.: Validation and intercomparison of global Leaf Area Index products derived from remote sensing data, Journal of Geophysical Research: Biogeosciences, 113, https://doi.org/10.1029/2007JG000635, 2008.

Gitelson, A., Gritz, Y., and Merzlyak, M. N.: Relationships between leaf chlorophyll content and spectral reflectance and algorithms for non-destructive chlorophyll assessment in higher plant leaves, Journal of Plant Physiology, 160, 271-282, https://doi.org/10.1078/0176-1617-00887, 2003.

Haboudane, D., Miller, J. R., Tremblay, N., Zarco-Tejada, P. J., and Dextraze, L.: Integrated narrow-band vegetation indices for prediction of crop chlorophyll content for application to precision agriculture, Remote Sensing of Environment, 81, 416-426, https://doi.org/10.1016/S0034-4257(02)00018-4, 2002.

Houborg, R., Anderson, M., and Daughtry, C.: Utility of an image-based canopy reflectance modeling tool for remote estimation of LAI and leaf chlorophyll content at the field scale, Remote Sensing of Environment, 113, 259-274, https://doi.org/10.1016/j.rse.2008.09.014, 2009.

Houborg, R., Anderson, M. C., Daughtry, C. S. T., Kustas, W. P., and Rodell, M.: Using leaf chlorophyll to parameterize light-use-efficiency within a thermal-based carbon, water and energy exchange model, Remote Sensing of Environment, 115, 1694-1705, https://doi.org/10.1016/j.rse.2011.02.027, 2011.

Jay, S., Maupas, F., Bendoula, R., and Gorretta, N.: Retrieving LAI, chlorophyll and nitrogen contents in sugar beet crops from multi-angular optical remote sensing: Comparison of vegetation indices and PROSAIL inversion for field phenotyping, Field Crops Research, 210, 33-46, https://doi.org/10.1016/j.fcr.2017.05.005, 2017a.

Jay, S., Gorretta, N., Morel, J., Maupas, F., Bendoula, R., Rabatel, G., Dutartre, D., Comar, A., and Baret, F.: Estimating leaf chlorophyll content in sugar beet canopies using millimeter- to centimeter-scale reflectance imagery, Remote Sensing of Environment, 198, 173-186, https://doi.org/10.1016/j.rse.2017.06.008, 2017b.

Jiang, X., Zhen, J., Miao, J., Zhao, D., Shen, Z., Jiang, J., Gao, C., Wu, G., and Wang, J.: Newly-developed three-band hyperspectral vegetation index for estimating leaf relative chlorophyll content of mangrove under different severities of pest and disease, Ecological Indicators, 140, 108978, https://doi.org/10.1016/j.ecolind.2022.108978, 2022.

Keller, M., Schimel, D. S., Hargrove, W. W., and Hoffman, F. M.: A continental strategy for the National Ecological Observatory Network, The Ecological Society of America, 282-284, 2008.

https://doi.org/10.5194/essd-2022-277
Preprint. Discussion started: 16 August 2022

Kira, O., Linker, R., and Gitelson, A.: Non-destructive estimation of foliar chlorophyll and carotenoid contents: Focus on informative spectral bands, International Journal of Applied Earth Observation and Geoinformation, 38, 251-260, https://doi.org/10.1016/j.jag.2015.01.003, 2015.

Li, D., Chen, J. M., Zhang, X., Yan, Y., Zhu, J., Zheng, H., Zhou, K., Yao, X., Tian, Y., and Zhu, Y.: Improved estimation of leaf chlorophyll content of row crops from canopy reflectance spectra through minimizing canopy structural effects and optimizing off-noon observation time, Remote Sensing of Environment, 248, 111985, https://doi.org/10.1016/j.rse.2020.111985, 2020.

Li, J., Lu, X., Ju, W., Li, J., Zhu, S., and Zhou, Y.: Seasonal changes of leaf chlorophyll content as a proxy of photosynthetic capacity in winter wheat and paddy rice, Ecological Indicators, 140, https://doi.org/10.1016/j.ecolind.2022.109018, 2022.

Li, Y., Ma, Q., Chen, J. M., Croft, H., Luo, X., Zheng, T., Rogers, C., and Liu, J.: Fine-scale leaf chlorophyll distribution across a deciduous forest through two-step model inversion from Sentinel-2 data, Remote Sensing of Environment, 264, 112618, 2021.

Lu, X., Ju, W., Li, J., Croft, H., Chen, J. M., Luo, Y., Yu, H., and Hu, H.: Maximum Carboxylation Rate Estimation with Chlorophyll Content as a Proxy of Rubisco Content, Journal of Geophysical Research: Biogeosciences, 125, e2020JG005748, https://doi.org/10.1029/2020JG005748, 2020.

Luo, X., Croft, H., Chen, J. M., He, L., and Keenan, T. F.: Improved estimates of global terrestrial photosynthesis using information on leaf chlorophyll content, Global Change Biology, 25, 2499-2514, https://doi.org/10.1111/gcb.14624, 2019.

National Ecological Observatory, N.: Plant foliar traits (DP1.10026.001), National Ecological Observatory Network (NEON) [dataset], 10.48443/KMC7-8G05, 2022.

Piao, S., Wang, X., Park, T., Chen, C., Lian, X., He, Y., Bjerke, J. W., Chen, A., Ciais, P., and Tømmervik, H.: Characteristics, drivers and feedbacks of global greening, Nature Reviews Earth & Environment, 1, 14-27, https://doi.org/10.1038/s43017-019-0001-x, 2020.

Qian, B., Ye, H., Huang, W., Xie, Q., Pan, Y., Xing, N., Ren, Y., Guo, A., Jiao, Q., and Lan, Y.: A sentinel-2-based triangular vegetation index for chlorophyll content estimation, Agricultural and Forest Meteorology, 322, 109000, https://doi.org/10.1016/j.agrformet.2022.109000, 2022a.

Qian, X. and Liu, L.: Retrieving crop leaf chlorophyll content using an improved look-up-table approach by combining multiple canopy structures and soil backgrounds, Remote Sensing, 12, 2139, https://doi.org/10.3390/rs12132139, 2020.

Qian, X., Liu, L., Croft, H., and Chen, J. M.: Relationship between Leaf Maximum Carboxylation Rate and Chlorophyll Content Preserved across 13 Species, Journal of Geophysical Research: Biogeosciences, e2020JG006076, https://doi.org/10.1029/2020JG006076, 2021.

Qian, X., Liu, L., Chen, X., Zhang, X., Chen, S., and Sun, Q.: The global leaf chlorophyll content dataset over 2003–2012 and 2018–2020 derived from MERIS/OLCI satellite data [dataset], http://doi.org/10.25452/figshare.plus.20439351, 2022b.

Ryu, Y., Berry, J. A., and Baldocchi, D. D.: What is global photosynthesis? History, uncertainties and opportunities, Remote Sensing of Environment, 223, 95-114, https://doi.org/10.1016/j.rse.2019.01.016, 2019.

Scholl, V. M., Cattau, M. E., Joseph, M. B., and Balch, J. K.: Integrating National Ecological Observatory Network (NEON) airborne remote sensing and in-situ data for optimal tree species classification, Remote Sensing, 12, 1414, https://doi.org/10.3390/rs12091414, 2020.

Si, Y., Schlerf, M., Zurita-Milla, R., Skidmore, A., and Wang, T.: Mapping spatio-temporal variation of grassland quantity and quality using MERIS data and the PROSAIL model, Remote Sensing of Environment, 121, 415-425, https://doi.org/10.1016/j.rse.2012.02.011, 2012.

Simic, A., Chen, J. M., and Noland, T. L.: Retrieval of forest chlorophyll content using canopy structure parameters derived from multi-angle data: the measurement concept of combining nadir hyperspectral and off-nadir multispectral data, International Journal of Remote Sensing, 32, 5621-5644, https://doi.org/10.1080/01431161.2010.507257, 2011.

Sims, D. A. and Gamon, J. A.: Relationships between leaf pigment content and spectral reflectance across a wide range of species, leaf structures and developmental stages, Remote Sensing of Environment, 81, 337-354, https://doi.org/10.1016/S0034-4257(02)00010-X, 2002.

https://doi.org/10.5194/essd-2022-277
Preprint. Discussion started: 16 August 2022

Sun, J., Shi, S., Wang, L., Li, H., Wang, S., Gong, W., and Tagesson, T.: Optimizing LUT-based inversion of leaf chlorophyll from hyperspectral lidar data: Role of cost functions and regulation strategies, International Journal of Applied Earth Observation and Geoinformation, 105, 102602, 2021a.

Sun, J., Shi, S., Yang, J., Du, L., Gong, W., Chen, B., and Song, S.: Analyzing the performance of PROSPECT model inversion based on different spectral information for leaf biochemical properties retrieval, Isprs Journal of Photogrammetry and Remote Sensing, 135, 74-83, https://doi.org/10.1016/j.isprsjprs.2017.11.010, 2018.

Sun, Q., Jiao, Q., Liu, L., Liu, X., Qian, X., Zhang, X., and Zhang, B.: Improving the Retrieval of Forest Canopy Chlorophyll Content From MERIS Dataset by Introducing the Vegetation Clumping Index, IEEE Journal of Selected Topics in Applied Earth Observations and Remote Sensing, 14, 5515-5528, https://doi.org/10.1109/JSTARS.2021.3082621, 2021b.

Verhoef, W., Jia, L., Xiao, Q., and Su, Z.: Unified Optical-Thermal Four-Stream Radiative Transfer Theory for Homogeneous Vegetation Canopies, IEEE Transactions on Geoscience and Remote Sensing, 45, 1808-1822, https://doi.org/10.1109/TGRS.2007.895844, 2007.

Verrelst, J., Camps-Valls, G., Muñoz-Marí, J., Rivera, J. P., Veroustraete, F., Clevers, J. G. P. W., and Moreno, J.: Optical remote sensing and the retrieval of terrestrial vegetation bio-geophysical properties–A review, ISPRS Journal of Photogrammetry and Remote Sensing, 108, 273-290, https://doi.org/10.1016/j.isprsjprs.2015.05.005, 2015.

Wang, S., Li, Y., Ju, W., Chen, B., Chen, J., Croft, H., Mickler, R. A., and Yang, F.: Estimation of leaf photosynthetic capacity from leaf chlorophyll content and leaf age in a subtropical evergreen coniferous plantation, Journal of Geophysical Research: Biogeosciences, 125, e2019JG005020, https://doi.org/10.1029/2019JG005020, 2020.

Wu, C., Niu, Z., Tang, Q., and Huang, W.: Estimating chlorophyll content from hyperspectral vegetation indices: Modeling and validation, Agricultural and Forest Meteorology, 148, 1230-1241, https://doi.org/10.1016/j.agrformet.2008.03.005, 2008.

Xiao, J., Chevallier, F., Gomez, C., Guanter, L., Hicke, J. A., Huete, A. R., Ichii, K., Ni, W., Pang, Y., Rahman, A. F., Sun, G., Yuan, W., Zhang, L., and Zhang, X.: Remote sensing of the terrestrial carbon cycle: A review of advances over 50 years, Remote Sensing of Environment, 233, https://doi.org/10.1016/j.rse.2019.111383, 2019.

Xu, M., Liu, R., Chen, J. M., Liu, Y., Shang, R., Ju, W., Wu, C., and Huang, W.: Retrieving leaf chlorophyll content using a matrix-based vegetation index combination approach, Remote Sensing of Environment, 224, 60-73, https://doi.org/10.1016/j.rse.2019.01.039, 2019.

Yin, G., Verger, A., Descals, A., Filella, I., and Peñuelas, J.: A Broadband Green-Red Vegetation Index for Monitoring Gross Primary Production Phenology, Journal of Remote Sensing, 2022, 1-10, https://doi.org/10.34133/2022/9764982, 2022.

Zarco-Tejada, P. J., Hornero, A., Beck, P. S. A., Kattenborn, T., Kempeneers, P., and Hernández-Clemente, R.: Chlorophyll content estimation in an open-canopy conifer forest with Sentinel-2A and hyperspectral imagery in the context of forest decline, Remote Sensing of Environment, 223, 320-335, https://doi.org/10.1016/j.rse.2019.01.031, 2019.

Zarco-Tejada, P. J., Berjón, A., López-Lozano, R., Miller, J. R., Martín, P., Cachorro, V., González, M. R., and De Frutos, A.: Assessing vineyard condition with hyperspectral indices: Leaf and canopy reflectance simulation in a row-structured discontinuous canopy, Remote Sensing of Environment, 99, 271-287, https://doi.org/10.1016/j.rse.2005.09.002, 2005.

Zhang, Y., Chen, J. M., and Thomas, S. C.: Retrieving seasonal variation in chlorophyll content of overstory and understory sugar maple leaves from leaf-level hyperspectral data, Canadian Journal of Remote Sensing, 33, 406-415, https://doi.org/10.5589/m07-037, 2007.

Zhang, Y., Chen, J. M., Miller, J. R., and Noland, T. L.: Leaf chlorophyll content retrieval from airborne hyperspectral remote sensing imagery, Remote Sensing of Environment, 112, 3234-3247, https://doi.org/10.1016/j.rse.2008.04.005, 2008.

Zhang, Y., Hui, J., Qin, Q., Sun, Y., Zhang, T., Sun, H., and Li, M.: Transfer-learning-based approach for leaf chlorophyll content estimation of winter wheat from hyperspectral data, Remote Sensing of Environment, 267, 112724, https://doi.org/10.1016/j.rse.2021.112724, 2021.